1.B Implementation of Power Balance on OMEGA

The stringent requirements for the irradiation uniformity for laser fusion, as reviewed in the previous article, have been known for quite some time. We have spent a significant effort on improving the irradiation patterns of the individual laser beams at the target surface as well as their energy balance and various geometrical effects due to beam disposition, pointing, and focusing.[1] In the process we have shown significant improvement in the laser performance with respect to overall (time-integrated) intensity distributions on target. In the area of irradiation patterns on target, the implementation of distributed (random) phase plates in each of the 24 high-power laser beams on OMEGA has shown, through the evaluation of equivalent-target-plane distributions, a decrease in the on-target nonuniformities by about a factor of 5.[2] In balancing the energy of the incident beams, which requires compensating for the varying performance of each of the 24 third-harmonic conversion crystals by adjusting the incident, 1054-nm laser energy, we have traditionally been able to maintain an on-target UV energy balance of ~6% rms. Regardless of these accomplishments, computational analysis of our recent high-density campaign has shown that there must be additional sources of nonuniformity that had not been previously considered.

We now believe that an important factor has been a time-varying illumination nonuniformity on target resulting from an inadequate power balance, i.e., the requirement that the instantaneous 351-nm power produced by the crystals balances at all times during the laser pulse. It is important to realize that good energy balance does not guarantee good power balance; for example, when the UV energy balance on previous targets was measured to be a modest 6% rms, the actual power imbalance, as will be shown later in this article, could have easily been in excess of 20%–30% rms. (Furthermore, power balance out of the crystals will not ensure intensity balance on target if the spot sizes of the individual beams are not the same. Strong air turbulence in the beam path or large, laser *B*-integral effects are examples that can lead to intensity imbalance on target, even when the power out of the crystals is balanced. However, our use of distributed phase plates reduces the sensitivity to spot-size changes and changes in intensity distribution in the target plane compared to experiments carried out without phase plates.)

After realizing the possibility of large power imbalance on the OMEGA laser system, a system review identified two areas of concern. The first was the state of polarization in each beam upon entry into the third-harmonic conversion crystals. It was found that, on average, each beam behaved as if it was detuned by ~200 μrad. This problem was solved with the insertion of output polarizers after the final 90-mm rod amplifiers. The second problem was found in the manual procedure for obtaining energy balance. The alleviation of this problem required the installation of a system of photodiodes to monitor

the oscillator energy and a series of computer-controlled, motorized splitter wave plates to allow the movement of all wave plates to within 0.05°. The improved polarization into the third-harmonic conversion crystals and improved tuning procedures now allow for a 2%-rms deviation from the optimum performance (worst beam ~100 μrad detuned) and with the computerized wave-plate system in place, the OMEGA laser system can now routinely obtain UV energy balance in the range of 2%–3% rms.

Origins of Power Imbalance

Power imbalance due to different temporal pulse shapes of the individual beams can arise from beam-to-beam differences in nonlinear processes such as frequency conversion[3] and saturation of the laser amplifiers.[4] For our laser the latter is of minor importance. However, the time-integrated, as well as the time-dependent, third-harmonic conversion efficiencies are very sensitive to crystal alignment, polarization (angle of linearly polarized light relative to the crystal axes and the uniformity of polarization across the beam), phase front, crystal thickness, and intensity distribution at the input to the crystals, and, as such, influence the temporal shape of the UV output pulses. The problem is exacerbated if such imperfect crystal performance is compensated for by increasing the IR laser energy incident on the crystal.

The well-known dependence of the time-integrated third-harmonic energy conversion efficiency as a function of peak input intensity to the conversion crystals is shown in Fig. 37.8. In this figure we have assumed 16-mm-thick KDP crystals for the doubler and the tripler, an idealized "top-hat" near-field intensity distribution, and a Gaussian temporal pulse shape. Also shown in this figure are conversion efficiencies for different values of the tuning and polarization angles. The effects of these conversion curves on the output temporal pulse shapes have been recognized for a long time, but their full impact on actual laser-fusion experiments has become obvious only recently. Figures 37.9(a) and 37.9(b) show typical examples of the calculated output pulse shapes for different detuning angles on linear and logarithmic scales, respectively. Only the rising parts of the Gaussian pulses are shown in the figures; the IR input energies to the crystals were adjusted such as to yield constant blue output energies independent of the tuning conditions consistent with past experimental OMEGA practice.

From Fig. 37.8 we note that the conversion efficiencies for different 3ω tuning conditions differ significantly from each other only at incident IR intensities above a few tenths of a GW/cm^2. Temporal pulse-shape distortion due to crystal detuning occurs, therefore, only in this intensity regime (i.e., within approximately the top decade of the temporal pulse shape). In the small-signal conversion regime the UV pulse shape is always predictably narrowed relative to the input Gaussian pulse shape (i.e., the wings are steepened), while above the small-signal conversion regime detuned crystals always flatten the top of the UV pulse and in some cases can even lead to a dip near the peak-incident IR pulse.

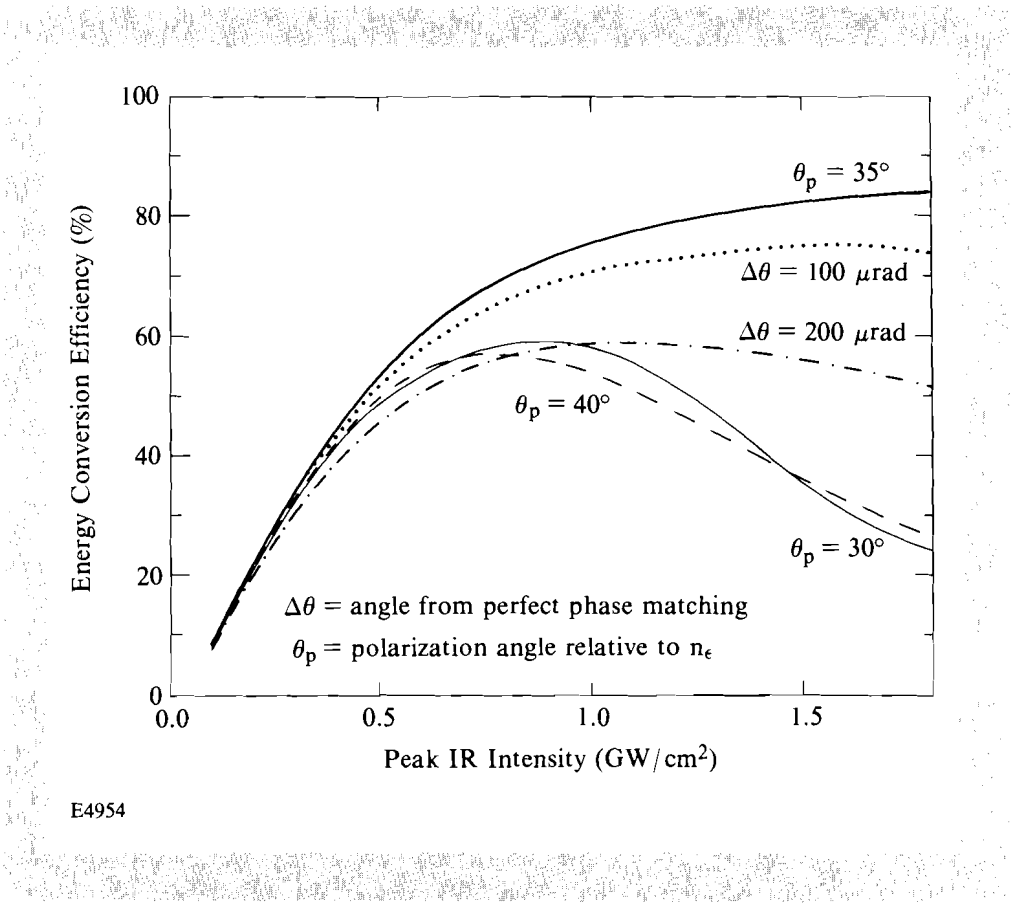

Fig. 37.8
Third-harmonic energy-conversion efficiency for type II-type II tripling in two 16-mm-thick KDP crystals for various tuning conditions: tripler tuning angle θ = 0, 100 μrad, and 200 μrad, and polarization angle θ_p = 30°, 33°, 35°, 37°, and 40° relative to the "*e*" axis of the input doubler crystal. [Note: the intensity axis scales as IL^2 and can therefore be applied easily to crystal pairs of different thicknesses provided the detuning angles are also scaled by θ_L.]

From Fig. 37.9(b) we see that while all the curves resemble each other at low intensities, they appear to be displaced in time. For laser fusion we require that the instantaneous deviations from the average intensity on target not differ by more than a few percent peak-to-valley at any time during the laser pulse. While OMEGA targets are illuminated by 24 beams, only four beams contribute significantly to the intensity on target at any particular point; thus, the 4% to 5% peak-to-valley illumination nonuniformity on target may relax to 8% to 10% peak-to-valley nonuniformity from beam to beam. Inspecting Fig. 37.9 one can easily see that, even for beams of equal energy, very large instantaneous intensity imbalances can occur between more-or-less perfectly frequency-converted beams. In Fig. 37.10 this is shown as $\Delta I/I$ as a function of time for the pulses shown in Fig. 37.9. The baseline for comparison in this figure was the perfectly tuned pulse (heavy line in Fig. 37.9); the worst instantaneous intensity deviation was determined for a crystal detuned by 200 μrad. Of course, larger detuning angles lead to even higher values of $\Delta I/I$. The bottom two curves in Fig. 37.10 are calculated for perfectly tuned tripling crystals but with 20% less IR input energy to the conversion crystals ($\sim$30% less UV crystal output). Curve 4 (second from bottom) has equal energy on target as a result of an assumed, rather extreme 30% difference in UV transport losses (Note: these do not represent OMEGA operating conditions). The bottom curve corresponds to a pulse whose energy on target is 30% less than nominal. The latter

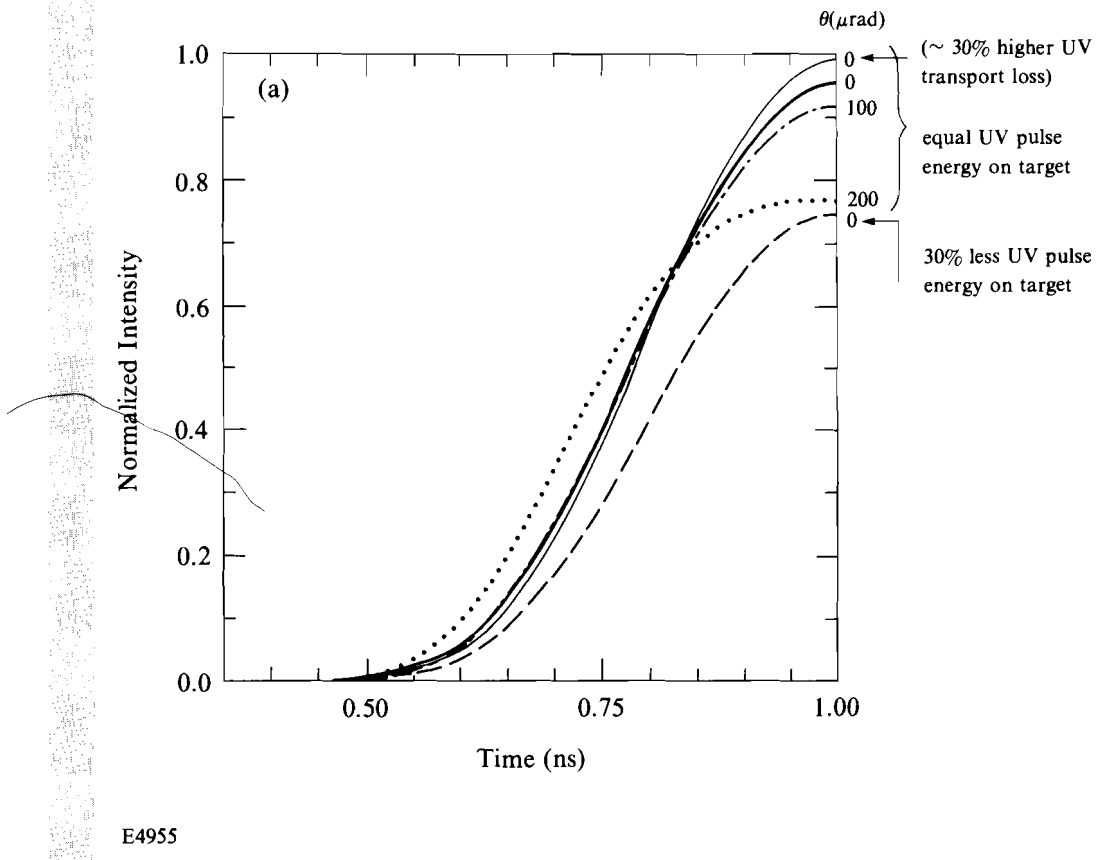

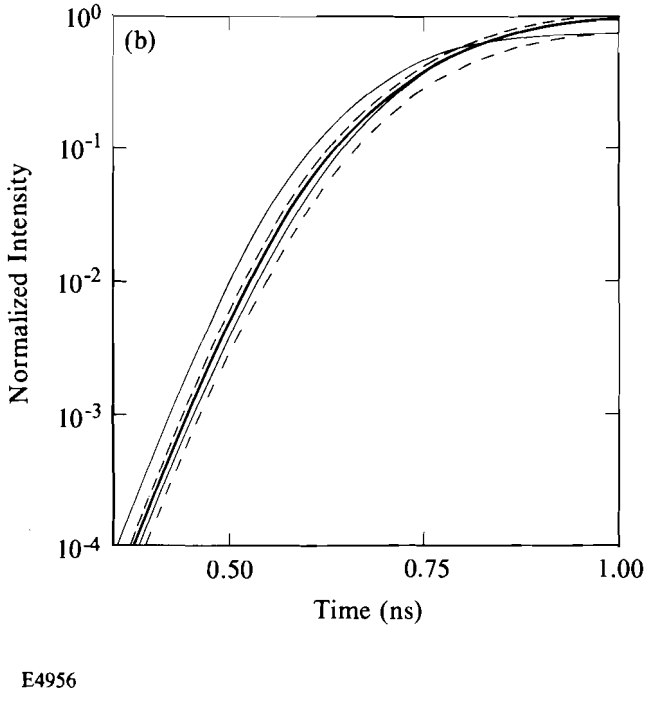

Fig. 37.9
Temporal pulse shapes of frequency-tripled Gaussian IR pulses of 500-ps FWHM and nominal IR peak intensity of 1 GW/cm^2. The angular detuning of the tripler crystal is indicated in μrad. All pulses (except the bottom curve) have been normalized to equal energy on target by compensating the IR input energy to the conversion crystals. The top curve for zero detuning is a mock-up for a beam whose transport losses between crystal and target area are arbitrarily assumed to be 30% less than for the other pulses while maintaining equal energy on target. The bottom curve in (a) has been calculated for 30% less UV energy on target, which is a typical peak-to-valley fluctuation in beam energy for a 6% to 8% beam-energy balance on target. In (b) the same pulse shapes are drawn on a logarithmic intensity scale.

pulse is consistent with a 5%- to 8%-rms beam-energy balance for which peak-to-valley excursions between individual beam energies typically reach 30%.

The $\Delta I/I$ curves of Fig. 37.10 show that the differential losses between the beam lines cannot be made up by simply adjusting the IR input energies to the crystals. This is, of course, a consequence of the changing third-harmonic conversion efficiency in the high-intensity regime rather than the transport losses that are relatively benign linear losses. On the other hand, large IR energy imbalances of ~20% peak-to-valley lead to instantaneous intensity imbalances in the UV of >50%, far in excess of the permissible levels for laser fusion. The situation becomes truly dramatic if one couples detuning problems with random beam energy fluctuations (5% to 8% rms has been typical for routine OMEGA operations) in which case instantaneous beam-intensity imbalances of several hundred percent can easily be realized.

Fig. 37.10
Time-dependence of the fractional intensity differences between the various pulses in Fig. 37.9. All curves are relative to the perfectly tuned case (second from top at the peak of the pulse in Fig. 37.9). We note that the maximum-intensity differences occur at about 1 FWHM from the peak of the IR pulse at a UV intensity of $\sim 10^{-3}$ of the peak.

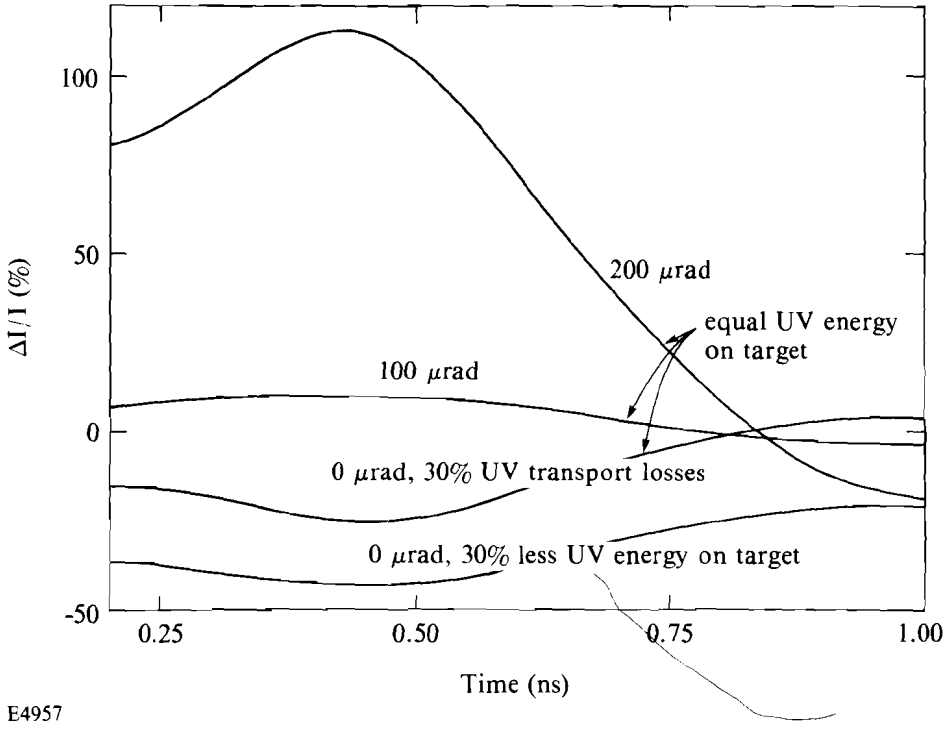

The worst instantaneous on-target intensity imbalance typically arises in the early part of the rising pulse (~1 IR FWHM from the peak of the pulse), at a time when the UV pulse intensity is $\sim 10^{-3}$ of its peak value (see Fig. 37.10). For laser fusion this corresponds to a time when only a small plasma corona surrounds the target, providing for little if any thermal smoothing to alleviate any on-target intensity

fluctuations. Hydrodynamic simulations of laser-fusion experiments have shown that targets nonuniformly irradiated at these early times with these low intensities never recuperate and consequently perform very poorly, even if the illumination uniformity improves later in the pulse.

In summary, careful examination of on-target $\Delta I/I$ values is essential for the success of laser fusion. Fortunately, most of the information concerning the pulse distortion can be obtained from examining the UV pulse shapes over the top one or two decades of intensity, provided that there are no beam-to-beam differences in the IR temporal pulse shapes. This is a relatively safe assumption for lasers using Gaussian temporal pulse shapes that do not operate too close to saturation. For other pulse shapes and lasers operating close to the saturated-gain regime, each beam has to be analyzed separately in the IR and UV unless a UV temporal-pulse diagnostic of very high dynamic range can be deployed on each beam.

OMEGA: Past Energy and Power Balance Performance

OMEGA's past approach to power balance was to achieve the best possible beam-to-beam energy balance. Typical values for the energy balance were 5% to 8% rms with peak-to-valley excursions roughly four times larger. As we have recently discovered, this limit on the energy balance was set by procedures and hardware as will be discussed later.

In order to analyze past OMEGA performance we have selected 70 shots from the high-density campaign, which ended in March 1988, where the selection criterion was an rms beam-energy balance of $\leq 8\%$. For this series of shots we have determined an average rms beam balance of $5\% \pm 1\%$ rms in the IR, with corresponding average peak-to-valley fluctuations of $20\% \pm 5\%$ rms. Interestingly, the average UV-beam-energy balance was only slightly higher at $6\% \pm 1\%$ rms with average peak-to-valley fluctuations of $24\% \pm 7\%$ rms.

Assuming perfectly tuned crystals, the preceding discussion on power balance indicates that the above peak-to-valley beam-energy excursions lead to intensity-dependent power imbalances far beyond the permissible limits for laser fusion. Including the actual frequency-conversion performance (actual/optimum conversion) of the crystals, the resulting peak-to-valley power imbalance for any of the analyzed OMEGA shots certainly exceeds 100% over a significant part of the pulse duration.

It is not possible to reconstruct exactly the values of the power imbalance on any one of these past OMEGA shots, but we can make reasonable estimates for the power imbalance from the known actual conversion efficiencies and the rather incomplete knowledge of pulse durations and shapes in either the IR or the UV. Thus, Fig. 37.11 shows a histogram of the relative conversion efficiencies for all these shots in terms of the differential percentage [(best conversion efficiency − worst)/best]. We note that on average the difference in conversion efficiencies between the best and worst converter is

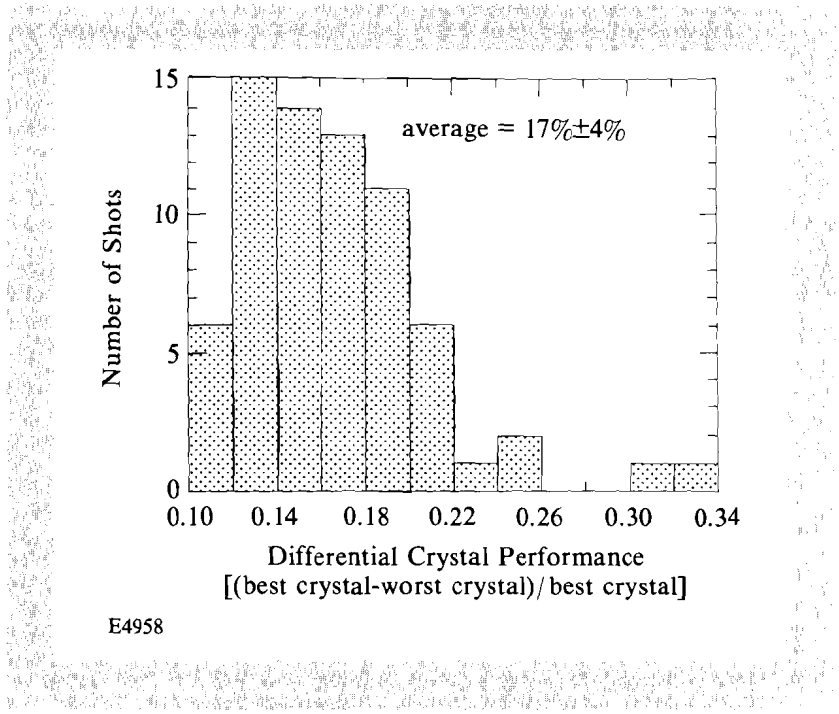

Fig. 37.11
Histogram of the fractional difference between the best and worst frequency converters in the 24-beam OMEGA system for a selection of 70 OMEGA shots of the high-density campaign. The selection criterion was better than 8%-rms beam-energy balance on target corresponding to 6%-average-rms energy balance. Assuming the best crystal to be perfectly tuned, a 20% difference in conversion performance corresponds roughly to 200-μrad detuning of the tripler crystal.

~17%. For 15% of the shots the differences in conversion efficiency were actually in excess of 20%. If we assume that the best converter corresponds essentially to a perfectly tuned crystal, Fig. 37.12 allows us to determine that the equivalent detuning angle for the average worst-performing crystal is 180 μrad$\pm$30 μrad. This angle is well beyond the standard 50-μrad angular-tuning accuracy for any of the crystals of OMEGA; but then it has long been noticed that the actual frequency-conversion performance of the crystals frequently lies 10% to 20% below the expected values. Simple polarization-angle detuning, as shown graphically in Fig. 37.13, could not explain this behavior as the angle of polarization was tuned to better than 1° for all crystals. However, scrutinizing the 70-shot series of OMEGA revealed an underestimate of the amount of depolarization across the beam area. This was caused by depolarization in the outer zones of the last 90-mm rod amplifier along with unrelated problems of input polarizers to the last amplifier, which were frequently removed for reasons of damage. In no case was there a final output polarizer directly preceding the conversion crystals.

Using Fig. 37.13 we can estimate the amount of depolarization, i.e., the amount of energy in the wrong (uncorrectable) polarization, needed to account for a 20% drop in conversion efficiency. Assuming the depolarization is spread uniformly across the beam area, a 3° rotation of the plane of polarization or approximately 0.3% (= $\sin^2 3°$) of the energy in the wrong state of polarization would suffice to account for the 20% decrease in frequency conversion. An alternative estimate is obtained if we concentrate the depolarization in the outermost 13% of the beam radius (25% of the beam area); in this case 4% of the beam energy in this area (polarization angle of ~24° instead of the optimum 35°) would be required to explain a 20% decrease in overall third-

Fig. 37.12
Angular tuning curves for the energy conversion to the third harmonic for different IR input intensities to the crystals (two 1.6-cm-thick KDP crystals).

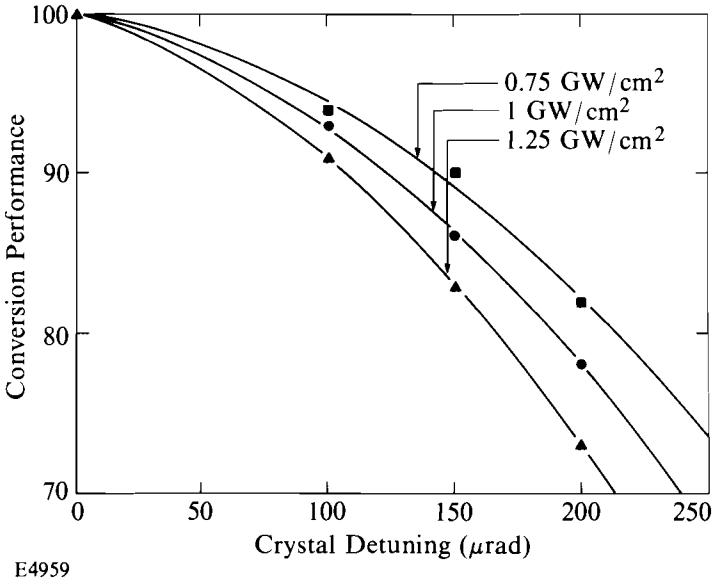

Fig. 37.13
Polarization-tuning curve for the third-harmonic energy-conversion efficiency at an IR input intensity to the conversion crystals of 1 GW/cm^2 (1.6-cm-thick KDP crystals). Also shown are the residual green at the output of the conversion crystals and the change in FWHM of the UV pulse as a function of the angle of the input polarization relative to the *e* axis of the frequency doubler. (Note that the UV pulse shape is a distorted Gaussian with the distortion increasing rapidly as the polarization angle is detuned from its optimum angle near 35°.)

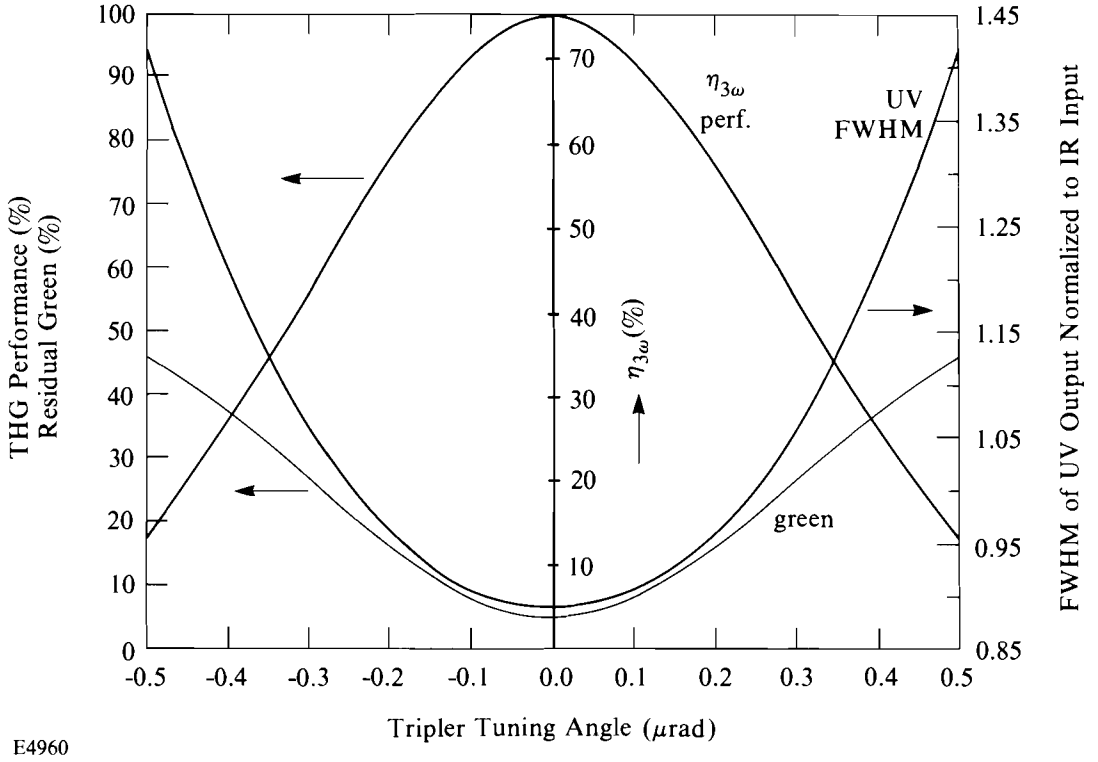

harmonic frequency conversion. If the depolarization were corrected through the introduction of a polarizer in the beam in front of the conversion crystals, the energy losses for these two model cases would be a negligible 0.3 and 1% overall!

The energy balance on OMEGA's 24 beams is carried out by manually rotating various half-wave and quarter-wave plates in front of polarization-sensitive beam splitters. The accuracy of these adjustments is now estimated to be $\sim 1°$ on average. Analysis of all the splitting areas has shown that the beam splitters do not behave like perfect polarizers but cause the output polarization from each beam splitter to be rotated significantly, requiring compensatory movements of subsequent wave plates. In addition, differential phase shifts between the "*s*" and "*p*" components lead to some ellipticity of the polarization after each beam splitter resulting in variable losses on subsequent polarizers in the beam. Imperfect knowledge of all these parameters and manual-setting accuracy of the 23 splitting wave plates in OMEGA made it impossible to achieve better than $\sim 5\%$-rms beam-energy balance as is easily verified through error propagation analysis.

To obtain a good estimate of the ultimate energy balance possible on OMEGA we have carried out a series of laser shots during which all laser parameters were held constant and a strict 30-min shot interval was maintained. The results are shown in Fig. 37.14 where the rms energy fluctuations for each beam are plotted along with their corresponding peak-to-valley excursions. We note that a 1%- to

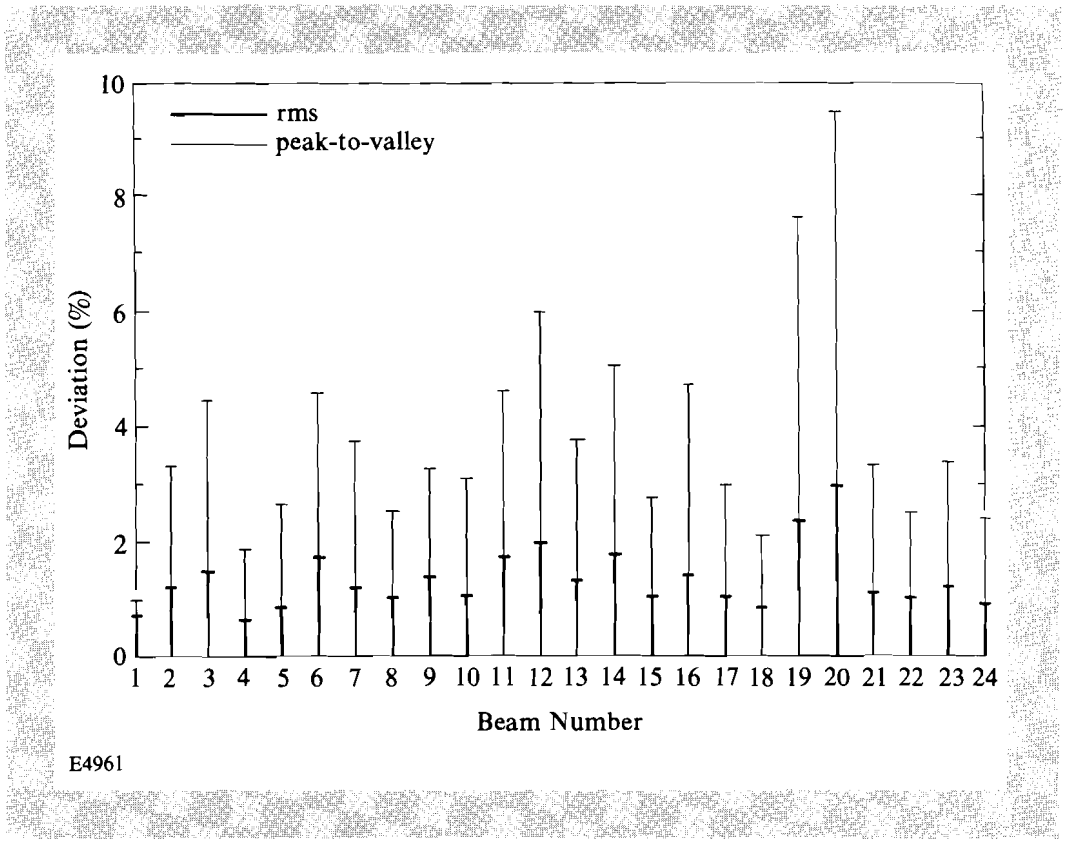

Fig. 37.14
Reproducibility of the beam energies in each of the 24 OMEGA beams for eight successive shots under identical operating conditions. No selection was made for misfires of individual flash lamps, which can probably account for some of the larger excursions (e.g., beam 20). The two error bars for each beam correspond to the percent rms and peak-to-valley fluctuations in each beam. From this data we estimate that the present limit to the beam balance lies around 1% to 1.5% rms or 4% to 5% peak-to-valley.

1.5%-rms beam-energy balance (3% to 4% peak-to-valley) should be obtainable on OMEGA. (The calibration accuracy and repeatability of the calorimetry system lies between 0.5% and 1%. Very stringent and frequent verification and control of the calorimetry as well as all the optics between the point of calorimetry and the target are required in order to maintain credible beam balance measurements.) However, such beam-energy-balance performance clearly cannot be obtained with past OMEGA practices.

OMEGA Improvements

1. Crystal Conversion

From the above discussion we concluded that the most important improvement regarding power balance comes from proper resetting of the polarization prior to frequency conversion. To this end we have now installed output polarizers after each of the final 90-mm rod amplifiers. The loss on these dielectric linear polarizers is expected to be mostly dominated by the residual 3% to 5% reflection of the transmitted "*p*" polarized light. We have also implemented improved methods for ascertaining proper tuning of the crystals through computerized performance checks. Our latest results indicate that it is now possible to keep the performance of the conversion crystals to within 2% rms (8% peak-to-valley) of the calculated optimum performance (further improvements are still possible). This implies that at present the worst-performing crystal could be detuned by ~ 100 μrad, or that the near-field intensity distributions of the various beams at the crystals cause the energy-conversion efficiencies to vary by up to 8%. Our present results are most likely due to a combination of both effects and the effects due to slight variations in crystal thicknesses.

2. Beam-Energy Balance

To improve the beam-energy balance on OMEGA we have implemented a system of photodiodes at the output of OMEGA that can monitor the oscillator output energy at that location. When these diode signals are normalized to high-energy, full-system shots, balancing the output energies of all 24 beams can proceed using only the oscillator. Furthermore, installation of motorized splitter wave plates allows the movement of all wave plates with accuracies of $\sim 0.05°$, well beyond the requirements. This system is now operational and yields 2%- to 3%-rms beam-energy balance within two iterations. A reduction of this value to 1% to 1.5% rms is possible provided failures of individual flash lamps are properly identified and eliminated.

Summary

The time-varying illumination nonuniformity caused by power imbalance has been identified as a problem on the OMEGA laser system. Correction of power imbalance required the insertion of output polarizers in each beam and the implementation of computer-controlled motorized splitter wave plates throughout the system. With these modifications in place, we are able to control the third-harmonic conversion in each beam to within 2% of the calculated optimum and can routinely maintain beam-energy balance at 2% to 3% rms.

Appendix

During the course of analysis of the data presented here we have found some convenient analytic approximations to a number of second- and third-harmonic energy conversion and tuning curves. This has significantly facilitated the tuning of the 24 pairs of conversion crystals in OMEGA and may help others doing research in the field of frequency conversion. These analytic approximations were based on computer calculations (MIXER[5]) for the harmonic conversion assuming a Gaussian temporal pulse shape and a top-hat spatial-intensity profile incident on the conversion crystals.

Figure 37.15 shows the calculated points and the analytic approximations for the second- and third-harmonic energy-conversion curves, while Figs. 37.16 and 37.17 show the second- and third-harmonic tuning curves and their best-fit Gaussian approximations. The Gaussian fits are accurate down to $<10\%$ of the peak of the conversion curves. The half-widths of the Gaussian are intensity dependent as shown in Fig. 37.18. Unfortunately, no satisfactory fits were found for the polarization tuning curves, with the best results shown in Fig. 37.19. Figures 37.16, 37.17, and 37.19 are all normalized to unity corresponding to our earlier definition of crystal performance. The actual value of the conversion at the peak of the tuning curves can be read from Fig. 37.15. The abscissae in these figures have been adapted to conveniently reflect the applicable scaling laws for the conversion efficiencies. The third-harmonic conversion and tuning curves assume equal crystal thicknesses for the second-harmonic and third-harmonic (MIXER) crystals.

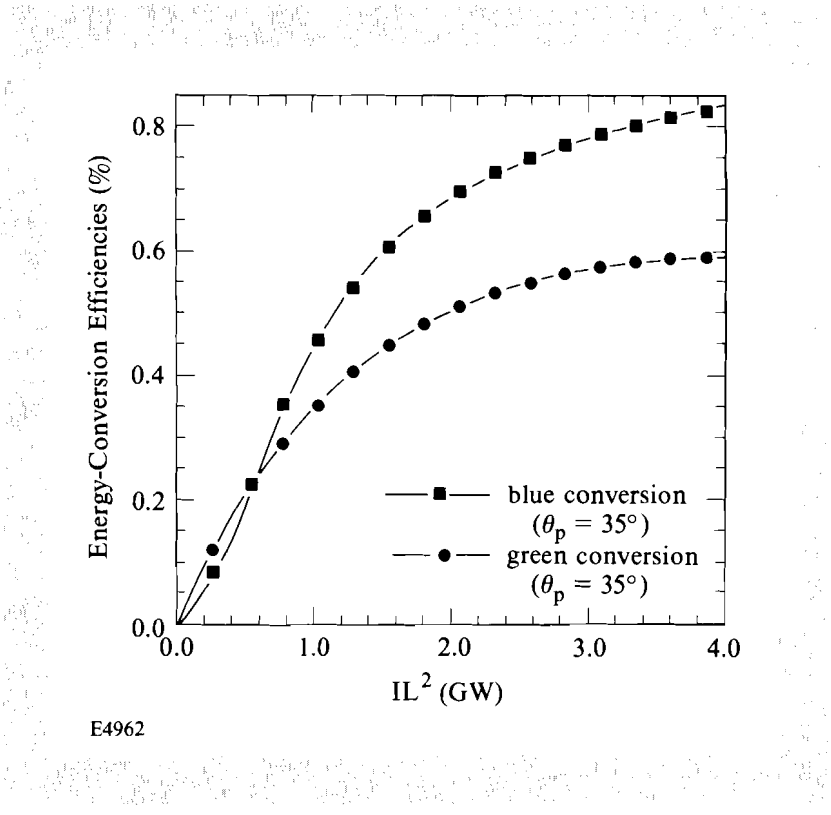

Fig. 37.15
Second- and third-harmonic energy-conversion curves for Gaussian temporal pulses and top-hat spatial intensity profiles as calculated by the simulation code MIXER[5] and their analytical best-fits. $\eta_{sh} = 82.94\ [1 - \exp(-0.624x + 0.0785x^2)]$; $\eta_{th} = 85.91\ [1 - \exp(-1.41x^2 + 0.869x^3 - 0.223x^4 + 0.0202x^5)]$, where $x = IL^2$ in GW, I is the IR intensity at the crystal input face, and L is the length of each of the two conversion crystals. The choice of IL^2 for the abscissa reflects the scaling law for the conversion efficiencies. The polarization at the input to the crystals is assumed to be at 35° with respect to the e axis of the doubler.

Fig. 37.16
Second-harmonic tuning curves for the energy-conversion efficiency as calculated by the simulation code MIXER[5] for Gaussian temporal pulses and top-hat spatial-intensity profiles. The x axis reflects the θ_L scaling law for the conversion efficiency. The best-fit curves are Gaussians [$\eta_{sh} = \exp(-A_{sh}\, x^2)$, $x = \theta_L$ in μrad.cm], with the intensity-dependent parameter A_{sh} given in Fig. 37.18.

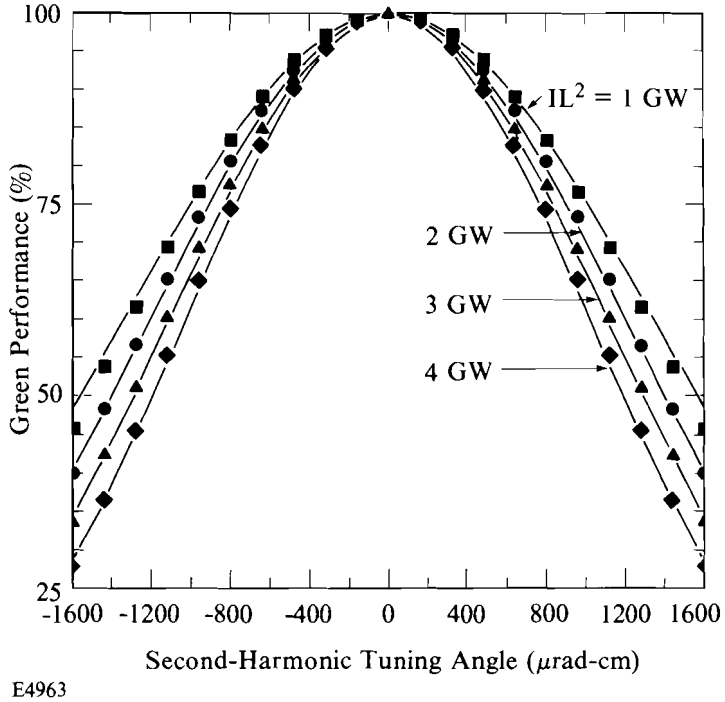

E4963

Fig. 37.17
Third-harmonic tuning curves for the energy-conversion efficiency as calculated by the simulation code MIXER[5] for Gaussian temporal pulses and top-hat spatial-intensity profiles. The x axis reflects the θ_L scaling law for the conversion efficiency. The best fit curves are Gaussians [$\eta_{th} = \exp(-A_{th}\, x^2)$, $x = \theta_L$ in μrad.cm], with the intensity-dependent parameter A_{th} given in Fig. 37.18.

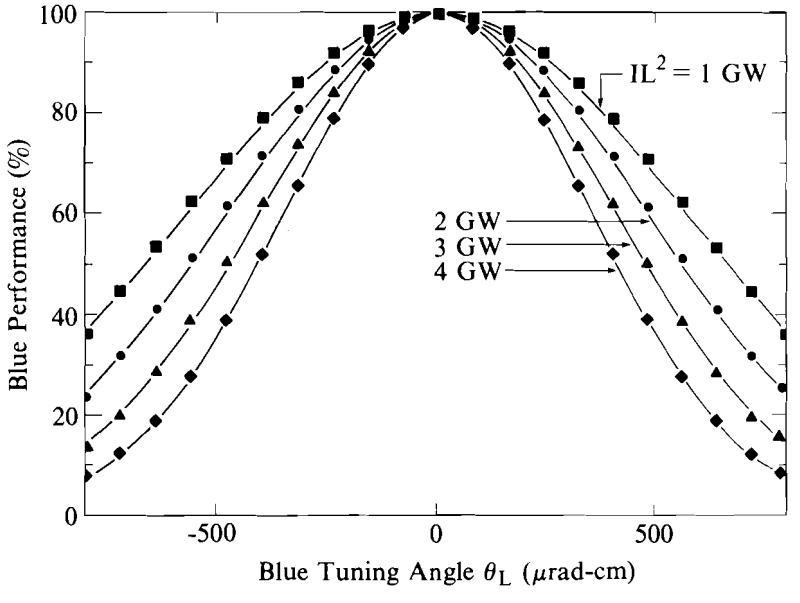

E4964

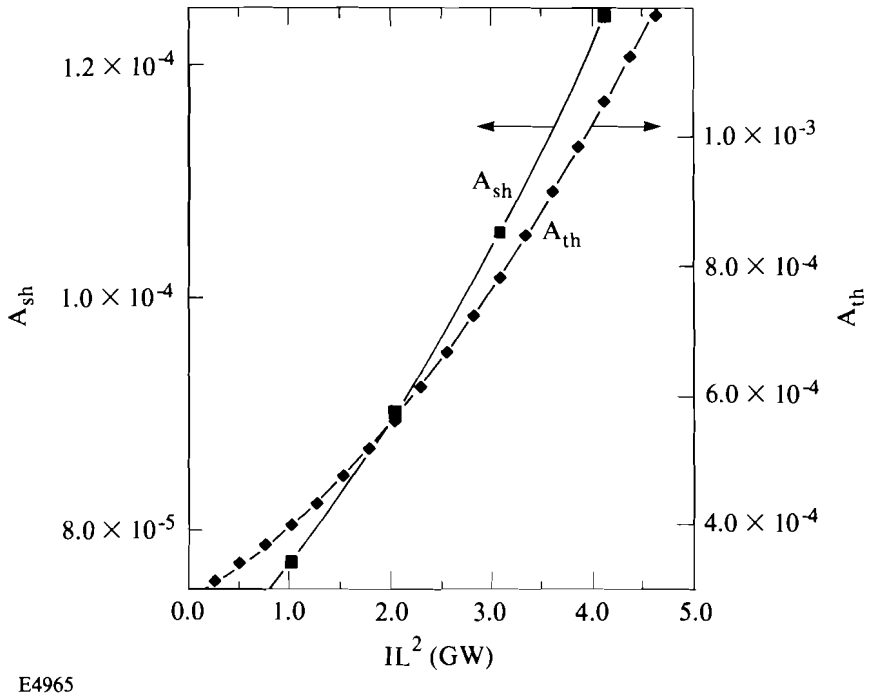

Fig. 37.18
Intensity dependence of the parameter A ($1/e$-widths = $1/\sqrt{A}$) of the Gaussian best fits for the second- and third-harmonic tuning curves of Figs. 37.16 and 37.17. $A_{sh} = 3.38 \times 10^{-6}x^2 + 8.59 \times 10^{-6}x + 2.62 \times 10^{-5}$, $A_{th} = 6.09 \times 10^{-4}x^2 + 8.93 \times 10^{-4}x + 1.11 \times 10^{-4}$, where $x = IL^2$ in GW as in Fig. 37.15.

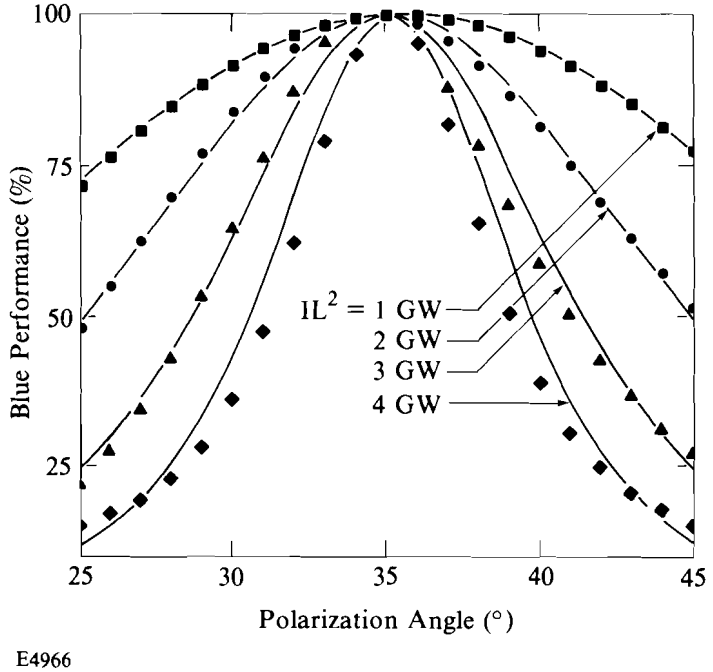

Fig. 37.19
Polarization-tuning curves for third-harmonic generation as calculated by the simulation code MIXER[5] for Gaussian temporal pulses and top-hat spatial-intensity profiles. The fitted curves shown in this figure are relatively poor fits but they are useful in certain applications. The analytic form of the best fits shown is $\eta_{th} = \exp(1/\{1+[(x-35)/x_p]^2\})$, where $x_p = 2.47x^2 - 21.5x + 57.5$, $x = IL^2$ in GW.